analytical chemistry

Article

Cite This: *Anal. Chem.* 2019, 91, 3681−3686

pubs.acs.org/ac

Novel $Ru(bpy)_2(cpaphen)^{2+}$/TPrA/TiO_2 Ternary ECL System: An Efficient Platform for the Detection of Glutathione with Mn^{2+} as Substitute Target

Rui Zhang,[†] Xia Zhong,[†] An-Yi Chen, Jia-Li Liu, Sheng-Kai Li, Ya-Qin Chai, Ying Zhuo,* and Ruo Yuan

Key Laboratory of Luminescent and Real-Time Analytical Chemistry (Southwest University), Ministry of Education, College of Chemistry and Chemical Engineering, Southwest University, Chongqing 400715, P. R. China

Supporting Information

ABSTRACT: A sensitive electrochemiluminescence (ECL) biosensor was developed for glutathione (GSH) detection based on a novel $Ru(bpy)_2(cpaphen)^{2+}$/TPrA/TiO_2 ternary ECL system with Mn^{2+} as substitute target for signal amplification. Specifically, the TiO_2 nanoneedles (TiO_2 NNs) were used as the coreaction accelerator for the first time to promote the oxidation process of coreactant tripropylamine (TPrA) in the anode and significantly increase the ECL signal of $Ru(bpy)_2(cpaphen)^{2+}$ for an amplified initial signal. Meanwhile, a novel target conversion strategy for GSH was developed by reducing MnO_2 nanosheets to Mn^{2+} as a substitute target, which played the role of a coenzyme factor for cleaving DNA double strands intercalated with $Ru(bpy)_2(cpaphen)^{2+}$ to markedly weaken initial signal. As a result, the novel "on−off" biosensor achieved a sensitive detection of GSH range from 5 μM to 215 μM with a detection limit of 0.33 μM. Importantly, the proposed strategy enriched the application of Ru complex and TPrA ECL system in bioanalytical applications, and provided a new signal amplification strategy for bioactive small molecules.

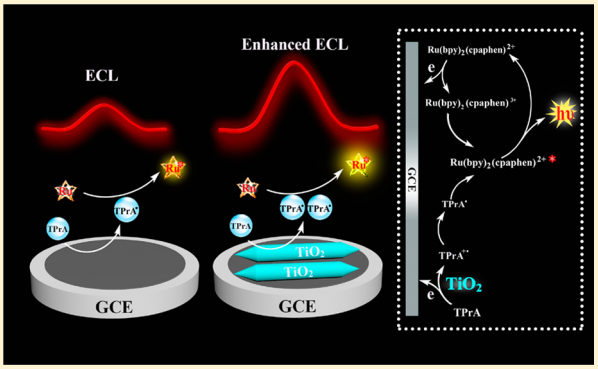

Electrochemiluminescence (ECL), an efficient analytical technique, has been widely applied in drug evaluation, environmental monitoring, disease diagnosis, and other fields owing to its high sensitivity, low background, and simple controllability.[1−3] Usually, the individual luminophore exhibited low ECL intensity due to its annihilation reaction.[4] In order to increase its response for analysis, the coreactant was introduced to form a binary system with luminophore for enhancing the ECL signal.[5,6] Generally, the excited state of the luminophore was generated through the reaction between the radical of luminophore and reactive intermediates of the coreactant produced by the electrochemical oxidation or reduction.[7,8] However, the reactive intermediates of the coreactant, as the key substance for the ECL intensity improvement, exhibited a relatively low generation rate on the electrode, which restricted the further improvement of the ECL signal. In our previous work, the coreaction accelerator was introduced into many traditional dual systems (luminophore/coreactant) to increase the oxidation or reduction rate of the coreactant for highly efficient ternary ECL systems construction.[9−11] It is well-known, the ruthenium (Ru) complex/tripropylamine (TPrA) system was one of the most popular ECL systems in analytical application and commercial ECL immunoassays with good photochemical stability, versatility and good water solubility.[12] Despite the exclusive popularity of the Ru complex/TPrA system, TPA suffered from several serious defects such as slow electrochemical oxidation rate as well as toxicity and volatility. Thus, it is of great significance to introduce a coreaction accelerator into the Ru complex/TPrA dual system, which can reduce the concentration of TPrA and obtain a higher sensitivity at the same time.[13] However, there was no report on the coreaction accelerator for the Ru complex/TPrA ECL system until now.

Titanium dioxide (TiO_2), as one of the most promising semiconductor nanomaterials, has attracted increasing interest in the fields of coatings, cosmetics, biosensors, photocatalysts, and batteries.[14−16] Owing to its low toxicity and good film forming properties, it was widely used as an immobilization matrix in the ECL field.[17] For example, TiO_2 nanoparticles not only used for recognition probes immobilization, but also the coreaction accelerator to promote the reduction of dissolved O_2 for the ECL intensity enhancement of silver cluster in the cathode, owing to the oxidizability of generated hole in TiO_2.[18] In this work, TiO_2 nanoneedles (TiO_2 NNs) were first introduced as a coreaction accelerator to accelerate the

Received: December 17, 2018
Accepted: January 30, 2019
Published: January 30, 2019

DOI: 10.1021/acs.analchem.8b05795
Anal. Chem. 2019, 91, 3681−3686

Scheme 1. (A) The Preparation Process of the Proposed ECL Biosensor; (B) The Conversion Process of GSH into Substitute Target Mn^{2+}; and (C) The Possible ECL Reaction Mechanism of (a) Ru Complex/TPrA Binary System and (b) Ru Complex/TPrA/TiO_2 Ternary System

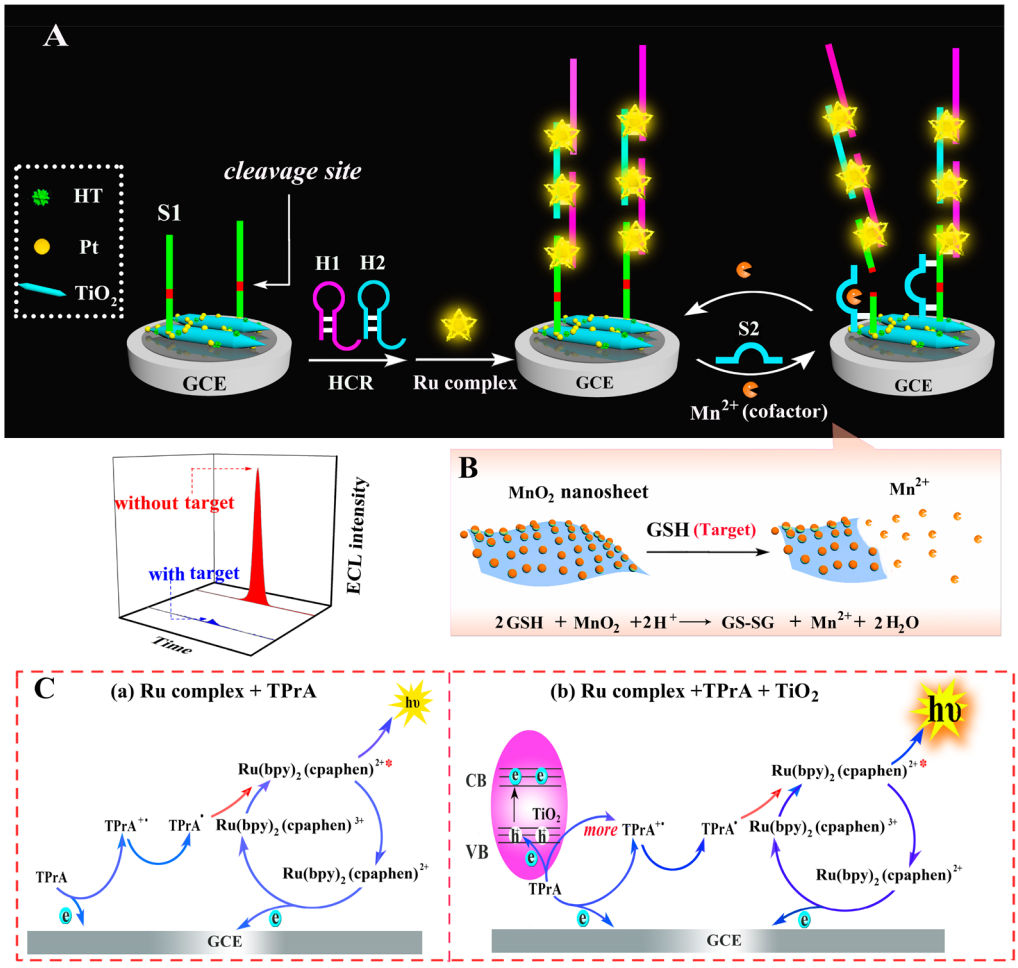

oxidation process of TPrA in the anode, and significantly increase the reaction rate between bis (2,2′-bipyridy) (5-amino-1,10-phenanthroline) ruthenium(II) (Ru(bpy)$_2$(cpaphen)$^{2+}$) and TPrA, resulting in a higher ECL response of Ru(bpy)$_2$(cpaphen)$^{2+}$.

Typically, with the aid of target conversion and nucleic acid amplification strategy, various detection methods of non-nucleic acid targets were achieved with high sensitivity.[19] However, the detection of non-nucleic acid targets was usually realized via the detection of the resultant DNA substitute targets converted by the target−aptamer complexes.[20] Glutathione (GSH) is a non-nucleic acid tripeptide containing sulfhydryl groups, and its expression is closely associated with many diseases such as psoriasis, AIDS, and cancer.[21,22] But the GSH aptamer has not been screened out up to now, which made it difficult to draw support from the nucleic acid amplification technology for GSH detection. Herein, a target conversion strategy was developed by transforming GSH detection to Mn^{2+} detection via dissolving MnO_2 nanosheets to Mn^{2+} owing to the reducibility of GSH. Thus, the Mn^{2+} was generated in proportionto a quantitative amount of GSH, which could act as a substitute target. With this target conversion, the Mn^{2+} further acted as the coenzyme factor for cleaving DNA double strands embedded with Ru(bpy)$_2$(cpaphen)$^{2+}$ to significantly weaken the initial signal and achieve a sensitive detection of GSH.

In this study, we combined the novel Ru(bpy)$_2$(cpaphen)$^{2+}$/TPrA/TiO_2 ternary ECL system and Mn^{2+} based target conversion strategy for the sensitive detection of GSH. The preparation processes and possible mechanism of the biosensor were depicted in Scheme 1. First, the glass carbon electrode (GCE) was coated with Pt nanoparticle modified TiO_2 NNs (Pt NPs@TiO_2 NNs) for the loading of stand 1 (S1) with cleavage point of Mn^{2+}. Then, the hairpain 1 (H1) was captured by S1 to trigger the hybridization chain reaction (HCR) for dsDNA structures generation on the electrode interface. Then, the ECL luminophore Ru(bpy)$_2$(cpaphen)$^{2+}$ was embedded into the long dsDNA structures to obtain a strong initial ECL as the "signal-on" state in the presence of coreaction accelerator (TiO_2 NNs). Meanwhile, the target GSH with different concentrations was incubated with MnO_2 nanosheets to obtain Mn^{2+} in the supernatant (abbreviated as *sample solution*). After the modified electrode was incubated with *sample solution* and stand 2 (S2), S2 bounded with the bottom (S1 with cleavage sites) of dsDNA structures and cleaved it in the assistance of Mn^{2+}. Finally, with the leaving of dsDNA structures intercalated with Ru(bpy)$_2$(cpaphen)$^{2+}$ on electrode interface, a "signal-off" state was obtained, and this biosensor realized a sensitive detection of GSH with a

DOI: 10.1021/acs.analchem.8b05795
Anal. Chem. 2019, 91, 3681−3686

detection limit of 0.33 μM. This strategy opened a new trail for the application of semiconductor materials in the field of ECL, and filled the gap in the application of the coreaction accelerator in Ru complex/TPrA system.

EXPERIMENTAL SECTION

Preparation of Pt NPs@TiO_2 NNs. The TiO_2 NNs were synthesized according to our previous report.[17] Pt NPs were modified on the surface of TiO_2 NNs to prepare the Pt NPs@TiO_2 NNs nanocomposite (the preparation of Pt NPs was supplied in Section 1.3 of the Supporting Information, SI). Briefly, 2 mL TiO_2 NNs and 50 μL PDDA (3%) were added into a 5 mL beaker with stirring for 12 h. After the product was collected by centrifuging and washing, 1 mL negatively charged Pt NPs was added dropwise with stirring for 7 h for adsorbing on the TiO_2 NNs functionalized with positively charged PDDA via electrostatic adsorption. Finally, the Pt NPs@TiO_2 NNs were obtained through washing with deionized water for three times after centrifugation, and further redispersed in 2 mL deionized water.

Fabrication of the Biosensor. The bare GCE was polished with alumina according to the previous study.[23] First, 10 μL Pt NPs@TiO_2 NNs was modified on the GCE and dried at 40 °C. Then, 10 μL S1 (2 μM) with amino groups was attached onto the Pt NPs@TiO_2 NNs surface overnight at 4 °C. After that, 1 mM HT was added onto the electrode for 2 h to block the nonspecific sites. Subsequently, the modified electrode was incubated with 10 μL mixed solution containing 2 μM H1 and 2 μM H2 for 2 h at room temperature. Ultimately, 10 μL $Ru(bpy)_2(cpaphen)^{2+}$ (2 mM) was incubated on the electrode for 7 h at room temperature.

Procedures of GSH Detection. 500 μL GSH solutions (10−430 μM) with different concentrations were mixed with the 500 μL MnO_2 nanosheets in the 1.5 mL-centrifuge tube (the preparation of MnO_2 nanosheets was supplied in the Section 1.4 of the SI). Then the mixture was shaken for 3 min at room temperature (see Figure S1 of the SI) and further centrifugated for 10 min at 10 000 rpm. 800 μL of the supernatant obtained after centrifugation was used as a *sample solution*. Subsequently, 10 μL mixture containing 5 μL S2 (2 μM) and 5 μL *sample solution* was cast onto the resultant electrode for 75 min. After that, the biosensor was measured in 2 mL PBS (pH 7.4) containing 10 mM TPrA with the ECL potential ranged from 0 to 1.25 V. Simultaneously, the ECL response was obtained at a scan rate of 300 mV/s.

Applications for GSH Determination in Human Serum Samples. One mL mixture containing 10-fold diluted fresh human serum sample, GSH solution with different conclusions (50 μM, 80 μM, and 100 μM) and 1 mM MnO_2 nanosheets were thoroughly mixed in 1.5 mL centrifuge tube and shaken for 4 min. Then, the mixture was centrifugated to obtain 800 μL supernatant for further detection. Finally, the measurements were carried out through the method as mentioned above (procedures of GSH detecion).

RESULTS AND DISCUSSION

Characterization of Nanomaterials. The scanning electron microscopy (SEM) was used to characterize the morphology of nanomaterials in this study. As shown in Figure 1A, the size distribution of synthesized TiO_2 NNs was reasonably uniform, and the lengths of needle-like particles were approximately 400 nm. Figure 1B showed the characterization of Pt NPs@TiO_2 NNs, which demonstrated that Pt NPs were uniformly distributed onto the TiO_2 NNs surface. Figure 1C and D shows the SEM and dynamic light scattering (DLS) characterization results of MnO_2 nanosheets, respectively. The lateral-diameter range of aslamellar MnO_2 nanosheets was 100−1100 nm with high specific surface area, which could provide a large number of reactive sites for GSH.

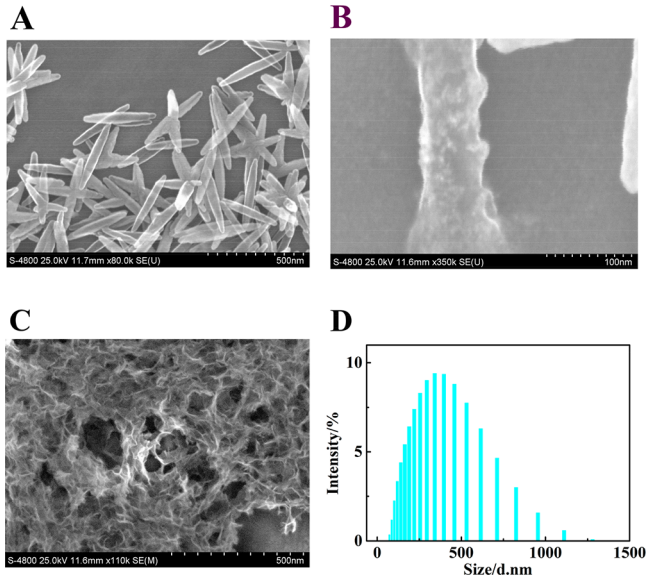

Figure 1. SEM images of (A) TiO_2 NNs. (B) Pt NPs@TiO_2 NNs. (C) the SEM and (D) DLS characterization of MnO_2 nanosheets.

Native Polyacrylamide Gel Electrophoresis (PAGE) Characterization. The PAGE assay was implemented to verify the feasibility of hybridization chain reaction (HCR) process and cleavage process. As depicted in Figure 2, the S1, H1, and H2 showed single band in lane *a*, *b*, and *c*, respectively. From lane *d* (the mixture of S1, H1, and H2), consecutive bands with much lower mobility were obtained, illustrating that the HCR process was carried out. Besides, lanes *e* and *f* showed the PAGE results for S1 + S2 and S1 + S2 + Mn^{2+} (the substitute target Mn^{2+} was obtained by reducing MnO_2 nanosheets with GSH), respectively. A new bright band appeared at the bottom of lane *f* (S1 + S2 + Mn^{2+}), which demonstrated that the cleavage process was carried out and

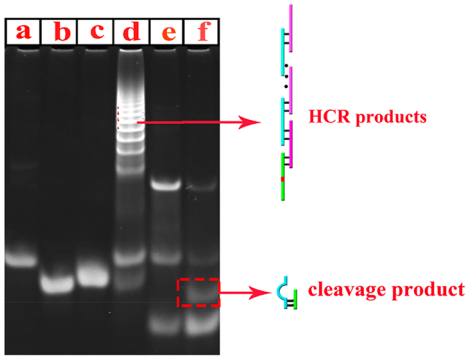

Figure 2. Native PAGE results of the samples: lane *a*, S1; lane *b*, H1; lane *c*, H2; lane *d*, S1, H1, H2; lane *e*, S1, S2; and lane *f*, S1, S2, sample solution containing Mn^{2+} (Mn^{2+} was obtained by reducing 1 mM MnO_2 nanosheets with 215 μM GSH). All of the concentrations of the oligonucleotides were 2 μM.

DOI: 10.1021/acs.analchem.8b05795
Anal. Chem. 2019, 91, 3681−3686

massive shorter sequences of S1 generated in the assistance of Mn^{2+}.

Possible Reaction Mechanism of Ru(bpy)$_2$(cpaphen)$^{2+}$/TPrA/TiO$_2$ system. The ECL measurements were made to explore the possible reaction mechanism. As shown in Figure 3A, the ECL intensity of TiO_2 NNs

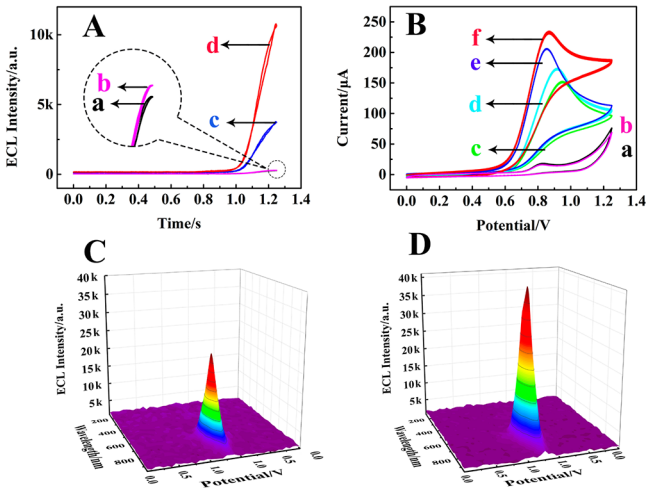

Figure 3. (A) The ECL intensity of bare GCE without (a) and with (b) TiO_2 NNs in Ru(bpy)$_2$(cpaphen)$^{2+}$ solution, the ECL intensity of bare GCE without (c) and with (d) TiO_2 NNs in the Ru(bpy)$_2$(cpaphen)$^{2+}$ + TPrA solution; (B) CVs of GCE without (a) and with (b) TiO_2 NNs in the Ru(bpy)$_2$(cpaphen)$^{2+}$ solution, CVs of GCE without (c) and with (d) TiO_2 NNs in the TPrA solution, CVs of bare GCE without (e) and with (f) TiO_2 NNs in the Ru(bpy)$_2$(cpaphen)$^{2+}$ + TPrA solution. The 3D ECL spectrum of bare GCE without (C) and with (D) TiO_2NNs/GCE in the Ru(bpy)$_2$(cpaphen)$^{2+}$ + TPrA solution. The concentration of Ru(bpy)$_2$(cpaphen)$^{2+}$ was 1.25 μM in ECL detection, ECL spectrum, and CV characterization (curve e and f); the concentration of Ru(bpy)$_2$(cpaphen)$^{2+}$ was 300 μM in curve a and b of CV characterization. The concentration of TPrA in ECL detection, CV characterization, and ECL spectrum was 5 mM, 10 mM, and 5 mM, respectively.

modified GCE (curve *b*) and bare GCE (curve *a*) exhibited no obvious difference in the Ru(bpy)$_2$(cpaphen)$^{2+}$ solution, indicating that TiO_2 NNs has no enhancement effect on the Ru(bpy)$_2$(cpaphen)$^{2+}$ without coreactant. When the bare GCE was measured in the Ru(bpy)$_2$(cpaphen)$^{2+}$/TPrA solution, the ECL intensity was increased to 4030.3 au owing to the presence of coreactant (curve *c*). After the TiO_2 NNs was modified onto the GCE surface, the ECL signal significantly increased to 10 870 a.u in Ru(bpy)$_2$(cpaphen)$^{2+}$/TPrA solution (curve *d*). Inspired by the mechanism of coreaction accelerator in ternary system,[24−26] we herein speculated that the TiO_2 NNs acted as a coreaction accelerator to react with TPrA for enhancing the ECL reaction rate between Ru(bpy)$_2$(cpaphen)$^{2+}$ and TPrA. To confirm this supposition, the cyclic voltammetry (CV) characterization was conducted with the cyclic potential scanning from 0 to 1.25 V. As exhibited in Figure 3B, the peak current of TiO_2 NNs modified GCE (curve b) and bare GCE (curve a) exhibited no distinct obvious change in Ru(bpy)$_2$(cpaphen)$^{2+}$ solution. When the GCE was measured in PBS (pH 7.4) solution containing TPrA, the oxidation current was about 152.4 μA (curve *c*). After TiO_2 NNs was modified onto the bare GCE, the oxidation current was significantly enhanced to 173.3 μA (curve *d*), suggesting that more TPrA was oxidized in this process. Besides, the current intensity of Ru(bpy)$_2$(cpaphen)$^{2+}$/TPrA with TiO_2 NNs modified GCE (curve *e*) was obviously stronger than that of GCE in Ru(bpy)$_2$(cpaphen)$^{2+}$/TPrA system (curve *f*), indicating that TiO_2 NNs could promote the oxidation rate of TPrA in the presence of Ru(bpy)$_2$(cpaphen)$^{2+}$. Therefore, the ECL and CV experimental results indicated that the TiO_2 NNs indeed play a role of coreaction accelerator for increasing the oxidation rate of TPrA and further enhancing the ECL intensity of Ru(bpy)$_2$(cpaphen)$^{2+}$ solution.

Subsequently, the 3D ECL spectra were characterized to further verify the conclusion. As depicted in Figure 3C, the maximum ECL emission wavelength of Ru(bpy)$_2$(cpaphen)$^{2+}$/TPrA solution was 625 nm, which was consistent with the previous report.[26] When the TiO_2 NNs were coated on GCE, the ECL response of Ru(bpy)$_2$(cpaphen)$^{2+}$/TPrA solution increased and the maximum emission wavelength was unchanged, indicating that the luminophore of the ECL system was still Ru(bpy)$_2$(cpaphen)$^{2+}$ (Figure 3D). According to the above results, it could be concluded that the TiO_2 NNs could increase the ECL intensity of Ru(bpy)$_2$(cpaphen)$^{2+}$/TPrA system and acted as the coreaction accelerator in this system.

On the basis of the above experimental results, the reaction mechanism of Ru(bpy)$_2$(cpaphen)$^{2+}$/TPrA/TiO_2 NNs is as follows. With the effect of the applied voltage, the electrons tunnelled from the valence band of TiO_2 to the conduction band,[27] and then immediately generated a hole in the valence band (eq 2), from which it was possible to gain electrons from species on the surface of TiO_2.[28] In this study, the hole of TiO_2 NNs obtained electrons from TPrA to accelerate the generation of $TPrA^{+\bullet}$ (eq 3b), resulting in more $TPrA^{\bullet}$ in unit time through the deprotonation process (eq 4). Hence, a significant enhancement of reaction rate between the $TPrA^{\bullet}$ and the Ru(bpy)$_2$(cpaphen)$^{3+}$ was obtained, and as a result the ECL intensity increased. Consequently, the reaction mechanism of this ECL system was expressed as detailed below:

$$Ru(bpy)_2(cpaphen)^{2+} - e^- \rightarrow Ru(bpy)_2(cpaphen)^{3+} \quad (1)$$

$$TiO_2 \xrightarrow{\text{voltage}} h^+ + e^- \quad (2)$$

$$TPrA - e^- \rightarrow TPrA^{+\bullet} \quad (3a)$$

$$TPrA + h^+ \rightarrow TPrA^{+\bullet} \quad (3b)$$

$$TPrA^{+\bullet} \rightarrow TPrA^{\bullet} + H^+ \quad (4)$$

$$Ru(bpy)_2(cpaphen)^{3+} + TPrA^{\bullet} \rightarrow Ru(bpy)_2(cpaphen)^{2+*} + \text{products} \quad (5)$$

$$Ru(bpy)_2(cpaphen)^{2+*} \rightarrow Ru(bpy)_2(cpaphen)^{2+} + h\nu \quad (6)$$

Analytical Performance of the GSH Biosensor. Under the optimized conditions (see SI Sections 2.1 and 2.2), the analytical performance of GSHbiosensor was shown in Figure 4. The changes in the ECL signals (ΔI_{ECL}) increased with the increasing concentrations of GSH, and a linear range of GSH was obtained from 5 to 215 μM with a detection limit of 0.33 μM (Figure 4A). As depicted in Figure 4B, the linear regression equation was conducted ΔI = 56.53 c (μM) − 119.86 with a correlation coefficient of 0.998. Compared with

DOI: 10.1021/acs.analchem.8b05795
Anal. Chem. 2019, 91, 3681−3686

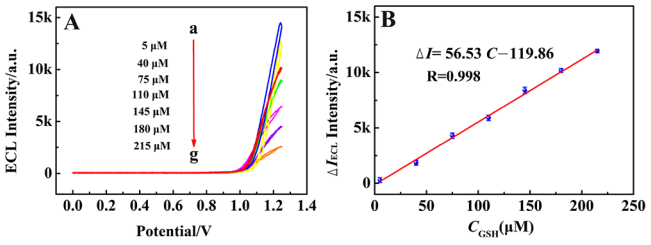

Figure 4. (A) ECL responses of the biosensor with different concentrations of GSH: (a) 5 μM, (b) 40 μM, (c) 75 μM, (d) 110 μM, (e) 145 μM, (f) 180 μM, and (g) 215 μM. (B) The calibration plot for GSH determination.

other reported assays, this proposed biosensor displayed excellent analytical performance with lower detection limit for the detection of GSH (Table S1 in the SI).

Selectivity and Stability of the Biosensor. Several kinds of interfering substances including ferric chloride ($FeCl_3$), potassium chloride (KCl), glycine (Gly), serine (Ser), histidine (His), tryptophan (Try), cysteine (Cys), and vitamin C (Vc) were employed to estimate the performance of the GSH biosensor to test the selectivity of the GSH biosensor. As displayed in Figure 5A, the ECL signal in the presence of 100

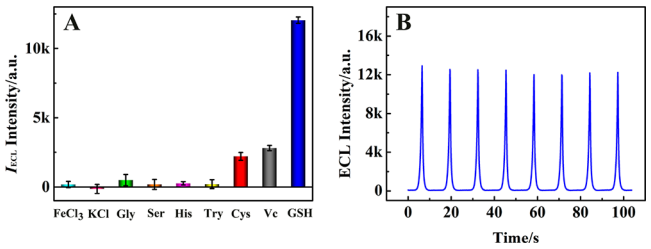

Figure 5. (A) The ΔI_{ECL} of the ECL biosensor with different interfering substances, $FeCl_3$, KCl Gly, Ser, His and Try 1 mM; Cys and Vc, 10 μM. (B) The ECL-time curve of the ECL biosensor under continuous scanning for 8 cycles in TPrA (10 mM) in the presence of 40 μM GSH.

μM GSH exhibited a remarkable change. Contrarily, the $FeCl_3$, KCl Gly, Ser, His, and Try showed no notable changes in the ECL signals (ΔI_{ECL}). Besides, Cys and Vc also caused a slight change of signal due to the their reducibility. However, the concentrations of Cys and Vc were far lower than GSH in biological systems,[29] indicating that this method was suitable for the selective detection of GSH in biological samples.

The continuous ECL scans of 8 cycles were monitored to study the stability of the biosensor (with 40 μM GSH) in 10 mM TPrA. As shown in Figure 5B, no significant change was observed with the continuous ECL signals, and the relative standard deviation (RSD) was 2.3%, indicating that the as-prepared biosensor showed a good stability.

GSH determination in human serum samples. To confirm the practicability in clinical analysis, this proposed biosensor was applied to detect GSH in fresh human serum. First, the background value of GSH concentration in 10-fold diluted serum was detected for three times. The obtained average value was 106.3 μM, which was close to the data of other works.[30] Subsequently, the human serum added different concentrations of GSH were detected in the same way as mentioned above. The analytical result (Table 1) indicated that this proposed biosensor was feasible for measuring GSH in human serum, which also possessed a broad prospect in reflecting the health status of living beings.

CONCLUSIONS

A novel biosensor was constructed for the sensitive determination of GSH by using TiO_2NNs as coreaction accelerator and Mn^{2+} as substitute target. This was the first report of coreaction accelerator in Ru complex/TPrA system, enriching the application of coreaction accelerator in the field of ECL. In addition, this work innovatively combined the Mn^{2+}-based target conversion and nucleic acid amplification strategy to detect GSH, which offered an efficient strategy for the detection of non-nucleic acid targets. Furthermore, this detection method provided a sensitive detection of GSH and has great potential in measuring the health status of the human body.

ASSOCIATED CONTENT

Supporting Information

The Supporting Information is available free of charge on the ACS Publications website at DOI: 10.1021/acs.analchem.8b05795.

Reagents and samples, instrumentation, preparation of Pt NPs, preparation of MnO_2 nanosheets, procedures of GSH detection, selection of the scan rate, optimal conditions for the ECL biosensor, CV characterization of the biosensor and comparison of different methods for GSH detection (DOC)

AUTHOR INFORMATION

Corresponding Author

*Tel.: +86 23 68253172. Fax: +86 23 68253172. E-mail: yingzhuo@swu.edu.cn (Y.Z.).

ORCID

Ya-Qin Chai: 0000-0003-4392-9592
Ying Zhuo: 0000-0002-4491-1186
Ruo Yuan: 0000-0003-3664-6236

Author Contributions

†These authors contributed equally to this work. All authors have given approval to the final version of the manuscript.

Notes

The authors declare no competing financial interest.

ACKNOWLEDGMENTS

This work was financially supported by the NNSF of China (21675130, 21775124, 21675129), and the Chongqing

Table 1. GSH Detection in Human Serum Samples

target	found in sample (μM)	add (μM)	total found (μM)	recovery (%) (n = 3)	RSD (%) (n = 3)
GSH		50	154.3 ± 5.2	96.0	3.4
	106.3 ± 3.9	80	184.0 ± 4.5	97.1	2.5
		100	210.3 ± 7.7	104.0	3.7

DOI: 10.1021/acs.analchem.8b05795
Anal. Chem. 2019, 91, 3681−3686

Research Program of Basic Research and Frontier Technology (cstc2018jcyjAX0546, cstc2017jcyjAX0230), the Fundamental Research Funds for the Central Universities (XDJK2018AA003, XDJK2018C041), China.

REFERENCES

(1) Cai, X. Li; Zheng, B.; Zhou, Y.; Younis, M. R.; Wang, F. B.; Zhang, W. M.; Zhou, Y. G.; Xia, X. H. *Chem. Sci.* **2018**, *9*, 6080−6084.
(2) Kim, J. M.; Jeong, S.; Song, J. K.; Kim, J. *Chem. Commun.* **2018**, *54*, 2838−2841.
(3) Zhang, R. Z.; Tong, F.; Yang, L. Q.; Adsetts, J. R.; Yan, T. H.; Wang, R. Y.; Ding, Z. F.; Wang, H. B. *Chem. Commun.* **2018**, *54*, 9897−9900.
(4) Richter, M. M. *Chem. Rev.* **2004**, *104*, 3003−3036.
(5) Miao, W. J.; Choi, J. P.; Bard, A. J. *J. Am. Chem. Soc.* **2002**, *124*, 14478−14485.
(6) He, Y. P.; Hou, S. F.; Yang, L. Q.; Zhang, F.; Zou, G. Z. *Chem. - Eur. J.* **2018**, *24*, 9592−9597.
(7) White, H. S.; Bard, A. J. *J. Am. Chem. Soc.* **1982**, *104*, 6891−6895.
(8) Carrara, S.; Arcudi, F.; Prato, M.; De Cola, L. *Angew. Chem.* **2017**, *129*, 4835−4839.
(9) Zeng, W. J.; Liao, N.; Lei, Y. M.; Zhao, J.; Chai, Y. Q.; Yuan, R.; Zhuo, Y. *Biosens. Bioelectron.* **2018**, *100*, 490−496.
(10) Ma, M. N.; Zhuo, Y.; Yuan, R.; Chai, Y. Q. *Anal. Chem.* **2015**, *87*, 11389−11397.
(11) Lei, Y. M.; Xiao, B. Q.; Liang, W. B.; Chai, Y. Q.; Yuan, R.; Zhuo, Y. *Biosens. Bioelectron.* **2018**, *109*, 109−115.
(12) Liu, Z. Y.; Qi, W. J.; Xu, G. B. *Chem. Soc. Rev.* **2015**, *44*, 3117−3142.
(13) Liu, X. Q.; Shi, L. H.; Niu, W. X.; Li, H. J.; Xu, G. B. *Angew. Chem.* **2007**, *119*, 425−428.
(14) Dugandžić, I. M.; Jovanović, D. J.; Mančić, L. T.; Milošević, O. B.; Ahrenkiel, S. P.; Šaponjić, Z. V.; Nedeljković, J. M. *Mater. Chem. Phys.* **2013**, *143*, 233−239.
(15) Chen, X. B.; Shen, S. H.; Guo, L. J.; Mao, S. S. *Chem. Rev.* **2010**, *110*, 6503−6570.
(16) Selcuk, S.; Selloni, A. *Nat. Mater.* **2016**, *15*, 1107−1112.
(17) Yang, X.; Yu, Y. Q.; Peng, L. Z.; Lei, Y. M.; Chai, Y. Q.; Yuan, R.; Zhuo, Y. *Anal. Chem.* **2018**, *90*, 3995−4002.
(18) Yu, Z. M.; Wei, X. H.; Yan, J. L.; Tu, Y. F. *Analyst* **2012**, *137*, 1922−1929.
(19) Li, D.; Song, S. P.; Fan, C. H. *Acc. Chem. Res.* **2010**, *43*, 631−641.
(20) Li, S. K.; Chen, A. Y.; Niu, X. X.; Liu, Z. T.; Du, M.; Chai, Y. Q.; Yuan, R.; Zhuo, Y. *Chem. Commun.* **2017**, *53*, 9624−9627.
(21) Yin, J.; Kwon, Y.; Kim, D.; Lee, D.; Kim, G.; Hu, Y.; Yoon, J.; Ryu, J.-H. *Nat. Protoc.* **2015**, *10*, 1742.
(22) Benhar, M.; Shytaj, I. L.; Stamler, J. S.; Savarino, A. *J. Clin. Invest.* **2016**, *126*, 1630−1639.
(23) Cai, W. R.; Zhang, G. Y.; Lu, K. K.; Zeng, H. Bo; Cosnier, S.; Zhang, X. J.; Shan, D. *ACS Appl. Mater. Interfaces* **2017**, *9*, 20904−20912.
(24) Lei, Y. M.; Wen, R. X.; Zhou, J.; Chai, Y. Q.; Yuan, R.; Zhuo, Y. *Anal. Chem.* **2018**, *90* (11), 6851−6858.
(25) Yang, S. S.; Jiang, M. H.; Chai, Y. Q.; Yuan, R.; Zhuo, Y. *ACS Appl. Mater. Interfaces* **2018**, *10* (44), 38648−38655.
(26) Liu, J. L.; Zhao, M.; Zhuo, Y.; Chai, Y. Q.; Yuan, R. *Chem. - Eur. J.* **2017**, *23*, 1853−1859.
(27) Zhou, Y.; Wang, H. J.; Zhuo, Y.; Chai, Y. Q.; Yuan, R. *Anal. Chem.* **2017**, *89*, 3732−3738.
(28) Yu, Z. M.; Wei, X. H.; Yan, J. L.; Tu, Y. F. *Analyst* **2012**, *137*, 1922−1929.
(29) Yu, F. B.; Li, P.; Wang, B. S.; Han, K. L. *J. Am. Chem. Soc.* **2013**, *135*, 7674−7680.
(30) Gao, W. Y.; Liu, Z. Y.; Qi, L. M.; Lai, J. P.; Kitte, S. A.; Xu, G. B. *Anal. Chem.* **2016**, *88*, 7654−7659.

DOI: 10.1021/acs.analchem.8b05795
Anal. Chem. 2019, 91, 3681−3686